OL | Organic Letters

pubs.acs.org/OrgLett

Letter

Tridentate Nickel(II)-Catalyzed Chemodivergent C–H Functionalization and Cyclopropanation: Regioselective and Diastereoselective Access to Substituted Aromatic Heterocycles

Ekta Nag, Sai Manoj N. V. T. Gorantla, Selvakumar Arumugam, Aditya Kulkarni, Kartik Chandra Mondal,* and Sudipta Roy*

Cite This: https://dx.doi.org/10.1021/acs.orglett.0c02138

Read Online

ACCESS | Metrics & More | Article Recommendations | Supporting Information

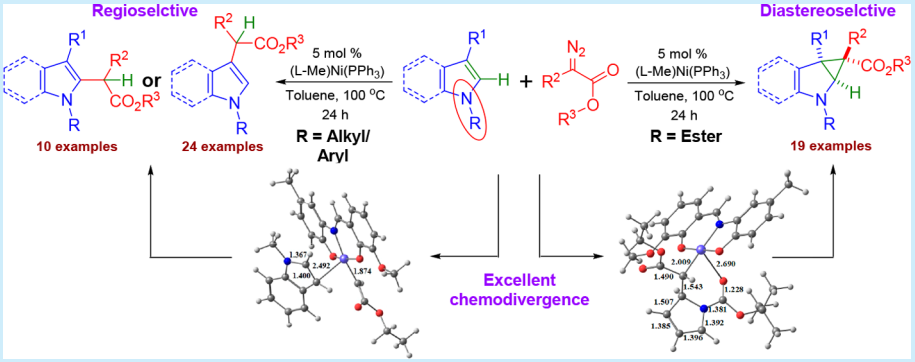

ABSTRACT: A Schiff-base nickel(II)-phosphene-catalyzed chemodivergent C–H functionalization and cyclopropanation of aromatic heterocycles is reported in moderate to excellent yields and very good regioselectivity and diastereoselectivity. The weak, noncovalent interaction between the phosphene ligand and Ni center facilitates the ligand dissociation, generating the electronically and coordinatively unsaturated active catalyst. The proposed mechanisms for the reported reactions are in good accord with the experimental results and theoretical calculations, providing a suitable model of stereocontrol for the cyclopropanation reaction.

Aromatic heterocycles, especially the functionalized indoles and pyrroles, are the prevalent structural motifs of a broad range of pharmaceutically active molecules.[1] There are ample examples of natural products and commercially available drugs containing these heterocycles as their core structures (Figure 1).[2] As a result, continuous efforts have been put forward to develop various stereoselective methods[3] for their syntheses,[4] including the enzyme-catalyzed[5] sustainable alternatives.

Late transition-metal phosphine complexes are well-known for exhibiting diverse catalytic properties.[6−8] However, their applications in catalytic carbene transfer reactions[9c] to heteroarenes are not documented so far.[9] Moreover, the harsh reaction conditions, and increased hazards of accumulation of the toxic heavy-metal wastes, especially for the large-scale industrial applications, very often limit their usage as catalysts. As a result, development of more abundant and cost-effective first-row transition-metal-based catalysts are on high demand.[10] Herein, we report the syntheses, characterization of a novel Schiff base-Ni(II)-phosphene complex **1** [(L-Me)Ni-(PPh_3); H_2L = ((E)-2-((2-hydroxy-3-methoxybenzylidene) amino)-4-methylphenol)] and its unprecedented catalytic application for the chemodivergent C–H functionalization and cyclopropanation of substituted indoles and pyrroles in the presence of various diazoesters.

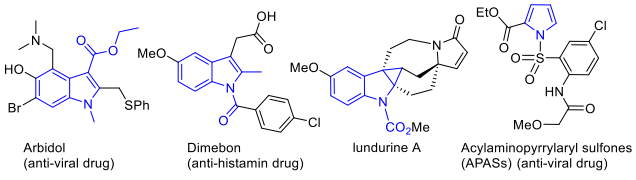

Figure 1. Representative bioactive molecules and natural products containing functionalized indole and pyrrole cores.

The air-stable, dark-brown block-shaped crystals of complex **1** (L-Me)Ni(PPh_3) were synthesized in 85% yield. **1** was characterized by single-crystal X-ray diffraction and various spectroscopic techniques, both in solid state and in solution (see the Supporting Information). The molecular structure of

Received: June 29, 2020

complex **1** contains a dideprotonated, tridentate Schiff base ligand $(L\text{-}Me)^{2-}$ coordinated to the Ni(II) center having a distorted square planar geometry. The PPh_3 moiety is coordinated to the metal center in a *trans* fashion with a Ni−P bond distance of 2.217(6) Å (see Figure 2, as well as

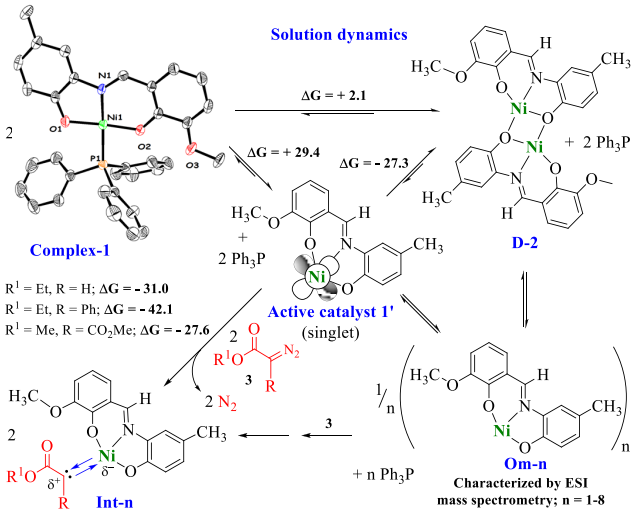

Figure 2. Molecular structure of complex **1** (top, left) and its solution dynamics. Generation of nickel(II)-carbenoid intermediate (**Int-n**). ΔG^{298} values are given in units of kcal/mol.

Figure S72 in the Supporting Information). The solution ^{31}P NMR spectrum of pure crystals of **1** exhibited two resonances: one at +10.9 ppm, corresponding to the coordinated phosphorus (Ni ← :PPh_3), and the other at −5.5 ppm, corresponding to the free PPh_3 (see Figures S16−S17 in the Supporting Information). The mass-spectrometric analysis of **1** in solution showed the presence of various oligomers [((L-Me)Ni)$_n$ (**Om-*n***), where n = 1−8] of the PPh_3-dissociated monomeric species **1′** [(L-Me)Ni], revealing the existence of solution dynamics (see the Supporting Information). To understand the bonding scenario of complex **1** and the reason behind the spontaneous dissociation of PPh_3 in solution, geometry optimization and NBO analysis were performed (see the Supporting Information for computational details). These studies led to the conclusion that the Ni−P bond in **1** mostly consists of noncovalent interaction (electrostatic, 61%), with a minor contribution from the orbital overlap and mixing (39%), resulting in a lower Ni−P bond dissociation energy ($-D_e$ = −29.8; $2\Delta G$ = +29.4 kcal/mol), which is comparable in magnitude with the dimerization energy (ΔG = −27.3 kcal/mol) of **1′** to produce **D-2** (Figure 2). This rationalizes the spontaneous ligand (PPh_3) dissociation from the nickel(II) center of complex **1**, creating the vacant coordination site in active catalyst **1′** (Figure 2).

Having these results in hand, we envisioned that the spontaneous dissociation (68%−75%, concluded by ^{31}P NMR studies) of PPh_3 from complex **1** when dissolved in organic solvents can create the vacant coordination site at the Ni center in **1′**, thereby facilitating the *in situ* generation of the nickel-carbenoid intermediate (**Int-*n***) in the presence of diazoester **3**, which can successively afford C−H functionalization or cyclopropanation of electron-rich *N*-heterocycles. We initiated the catalytic studies of complex **1**, choosing *N*-methylindole (**2a**) and ethyl diazoacetate (**3a**) as model substrates to react at room temperature, using DCM as a solvent in the presence of 5 mol % of complex **1** (see Table S2 in the Supporting Information, entry 1). To our delight, after 24 h, the C3-functionalized *N*-methylindole (**4a**) was obtained as a single regioisomer in 15% isolated yield. Inspired by this initial result, we moved to optimize the reaction condition (see Table S2). Having the optimized reaction conditions in hand, we turned our attention to probe the generality of the reaction by varying the diazoesters **3** (Scheme 1). In all of the cases, the

Scheme 1. Complex 1-Catalyzed C3−H Functionalization of Substituted Indoles[a]

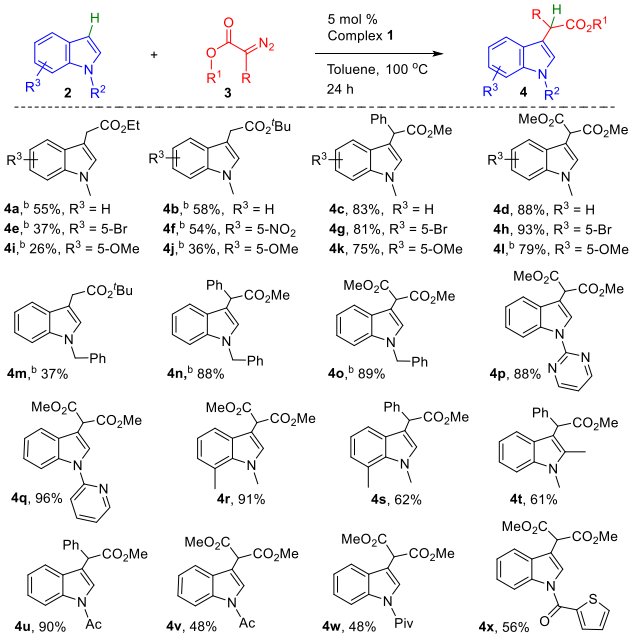

[a]Isolated yields for **4** are shown for the reactions performed at 100 °C for 24 h with 1 mmol of **2**, 1.5 mmol of **3**, and 5 mol % **1**, using toluene as the solvent. [b]Mixture of regioisomers (see the Supporting Information).

expected C3-functionalized *N*-methylindoles (**4b−4d**) were obtained in moderate to good isolated yields (58%−88%) and excellent regioselectivity. A much faster reaction with increased yield of C3-functionalized product **4d** (88%) was isolated exclusively when dimethyl 2-diazomalonate (**3e**) was employed (the corresponding nickel-carbenoid intermediate, **Int-3e** was observed to have the highest computed electrophilicity indices ω[11] of 5.08 eV, having the most electrophilic carbene center;[12] see Figures S50−S69 and Table S5 in the Supporting Information). Next, we moved to investigate the effect of different substituents at the adjacent phenyl ring of *N*-methylindole. Introduction of an electron-withdrawing Br-group at the 5-position of *N*-methylindole (**2b**), yielded the corresponding C3-functionalized product **4h** exclusively with an excellent yield of 93% when treated with **3e** (Scheme 1). However, introduction of an electron-donating OMe group at the 5-position of **2c** led to the formation of a mixture of both C3- and C2-functionalized products with various ratios in favor of the C3 product. This can be attributed to the increased electron density at both C3 and C2 positions (see the Supporting Information for computed molecular electrostatic potential (MEP) plot of **2c**[13a]). The presence of a Me group at the C7 and C2 positions of *N*-methylindoles afforded the

https://dx.doi.org/10.1021/acs.orglett.0c02138
Org. Lett. XXXX, XXX, XXX−XXX

corresponding C3-functionalized products exclusively (**4r**, 91%; **4s**, 62%; **4t**, 61%) when treated with the diazoester **3c**.

Next, we probed our reaction with electronically varied directing groups (DGs) attached to the N atom of indole in the presence of the most electron-deficient diazoester, dimethyl 2-diazomalonate (**3e**). Gratifyingly, in all of the cases, we observed the formation of the corresponding C3 functionalized indoles (**4l**−**4w**) exclusively in good to excellent yields (37%−96%). This regioselectivity can be attributed to the nucleophilic attack[14] of the indole derivatives (**2**) to the most electron-deficient $C_{carbene}$ of **Int-3e**, predominantly through the most electron-rich C3 center of **2** (see the Supporting Information[15a]). The presence of electron-donating DGs at the N atom of **2g** and **2h** afforded the corresponding C3-functionalized products **4p** and **4q** in 88% and 96% yields, respectively, when treated with **3e**. The robustness of the present method was established by conducting the reaction in a larger scale of 1.59 g of *N*-acetyl indole (**2l**, 10 mmol) and **3c** (15 mmol, 2.64 g). The desired product **4u** was isolated in 65% yield (see the Supporting Information).

Interestingly, under similar reaction conditions, *N*-methyl pyrrole (**2t**) yielded the corresponding C2-functionalized products (**5a**−**5j**) as the major products in the presence of various diazoesters (**3a**−**3e**) in good yields and moderate regioselectivity (see Scheme 2). Similar observation was found

Scheme 2. Complex 1-Catalyzed C2−H Functionalization of Substituted Pyrroles and Indoles[a]

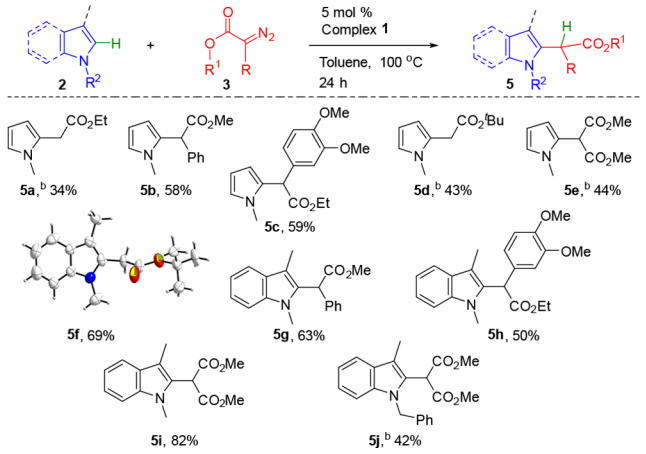

[a]Isolated yields for **5** are shown for the reactions performed at 100 °C for 24 h with 1 mmol of **2**, 1.5 mmol of **3**, and 5 mol % **1**, using toluene as the solvent. [b]Mixture of regioisomers (see the Supporting Information).

in the case of the 1,3-dimethylindole (**2k**), giving rise to the corresponding C2-functionalized products (**5f**−**5j**) in moderate to good yields (26%−82%).

Surprisingly, introduction of a stronger electron-withdrawing NO_2 group at the C5 position of *N*-methylindole (**2d**) produced the corresponding C3-functionalized product **4f** in 58% yield, along with the C2−C3 cyclopropanated product **4f′** as the minor product in 14% yield (see the Supporting Information). This result indicated that a relatively electron-poor C2−C3 π-system, as in **2d**, attributed by the negative mesomeric effect of the NO_2 group, may open up the possibility of cyclopropanation across the C2−C3 bond. The computed MEP plot of **2d** revealed the maximum electron density accumulation over the electron-withdrawing $-NO_2$ group at the C5 position, leading to the reduced electron densities around the C3−C2 positions (see the Supporting Information[15b]) with more double-bond character (see the Supporting Information[15c]). Overall, this result directed us toward a possible chemodivergent route to synthesize the C2/C3-cyclopropanated products by reducing the overall electron density over the C2═C3 double bond of the heteroarene **2** while reacting with diazoester **3** by introducing a suitable electron-withdrawing DG at the N atom.

As anticipated, changing the DG, R_2 of **2** from alkyl to the ester group under similar reaction conditions dramatically changed the course of the reaction (see the Supporting Information[15d]), leading to the formation of the corresponding C2/C3-cyclopropanated products **6** with excellent *exo*-diastereoselectivity (Scheme 3). The relative stereochemistry

Scheme 3. Complex 1-Catalyzed C2/C3 Cyclopropanation of Heteroarenes 2[a]

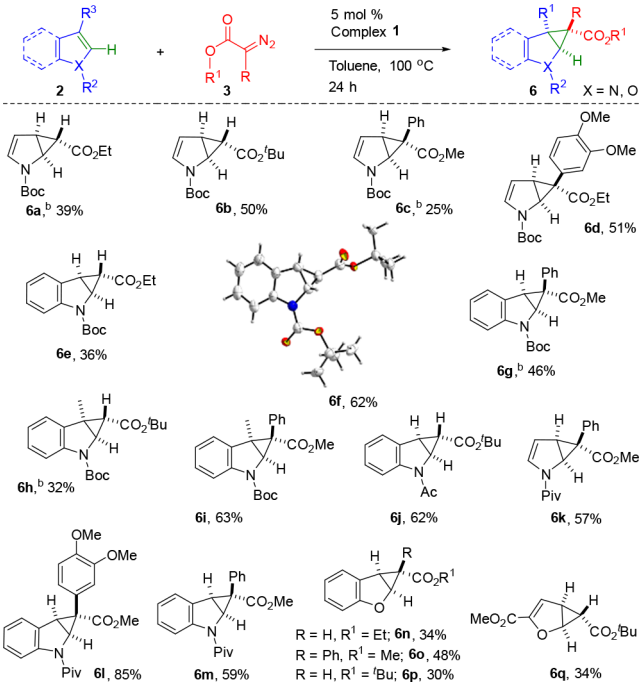

[a]Isolated yields of **6** are shown for the reactions performed at 100 °C for 24 h with 1 mmol of **2**, 1.5 mmol of **3**, and 5 mol % **1**, using toluene as the solvent. [b]Mixture of products (see the Supporting Information).

of **6** was unambiguously established by the single-crystal XRD studies of **6f** and **6r** (see the Supporting Information). When *N*-Boc pyrrole was separately treated with ethyl diazoacetate and methyl-2-diazo-2-phenylacetate, the corresponding cyclopropanated products **6a** (39%) and **6c** (25%) were isolated, along with the C2-functionalized products as the minor products (**6a′**, 12%; **6c′**, 10%). However, in the case of *tert*-butyl diazoacetate, the *exo*-cyclopropanated product **6b** (50%) was formed exclusively because of the increased steric bulk offered by the *tert*-butyl group. On the other hand, when *N*-Boc indole (**2q**) was treated with methyl-2-diazo-2-phenylacetate, the expected cyclopropanated product **6g** was isolated in 46% yield along with the corresponding C3-functionalized product (**6g′**) as the minor product (10%). This can be attributed to the more sterically hindered C2 position of **2q**, while coordinated to the Ni center with the carbonyl oxygen

https://dx.doi.org/10.1021/acs.orglett.0c02138
Org. Lett. XXXX, XXX, XXX−XXX

available for the nickel-carbenoid to attack. Under similar reaction conditions, benzofuran (**2s**) and methyl 2- and 3-furoates (**2u** and **2v**, respectively) afforded the corresponding cyclopropanated products **6n**–**6s** in moderate yields and diastereoselectivity.

It is noteworthy to mention that the reactivity of *N*-acetyl and *N*-pivaloyl indoles (**2g**, **2h**) was observed to be largely dependent on the specific diazoesters used as the reaction partner that decides the final products.[16]

The intermolecular competition experiment performed by treating **2a** with an equimolar mixture of the diazoesters **3b** and **3e** under similar reaction conditions led to the selective formation of **4d** (23%, Scheme 4). This result furnishes strong

Scheme 4. Competition Experiments[a]

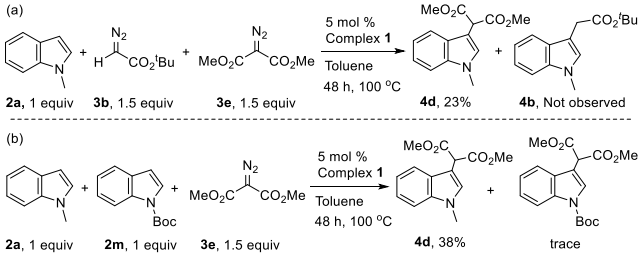

[a]Isolated yields are shown.

support in favor of the higher reactivity of **3e** over **3b** toward C3-H functionalization of **2a**. This can be attributed to the low lying LUMO of **Int-3e** (see the Supporting Information[15e]). Moreover, when an equimolar mixture of **2a** and **2m** was treated with 1.5 equiv of **3e**, the corresponding C3-functionalized product **4d** was isolated with only a trace amount of the C3-functionalized *N*-Boc derivative, showing the preference of the more-electrophilic nickel-carbenoid intermediate, **Int-3e**, toward the comparatively more electron-rich C3 position (see the Supporting Information[15f]) of **2a** than **2m**, producing **4d** in 38% yield.

To have an insight into the reaction mechanisms and origin for the present chemodivergence, NBO analysis were performed on **1′** and **Int-*n*** (see the Supporting Information). The Ni–$C_{carbene}$ bond of **Int-*n*** has been found to be of a donor–acceptor-type partial double bond (Ni → C and Ni ← C), which is slightly stronger (~10 kcal/mol) than the Ni–P bond in **1**. Accordingly, the computed bond dissociation energy (D_e) for Ni–$C_{carbene}$ bonds in **Int-*n*** was found to be higher, compared to that of the Ni–P bond in **1**, which favors the formation of **Int-*n*** (Figure 3).

Based on the experimental and theoretical investigations, we proposed that, upon dissociation of PPh_3 from **1**, the monomeric species **1′** (active catalyst) forms in the reaction mixture, which then generates **Int-*n*** *in situ* by reacting with the diazoester employed upon removal of the dinitrogen. Next, in the presence of the heteroarene containing electron-donating groups at the N atom (alkyl, aryl), **Int-*n*** forms a π-complex, **A** (Figure 3) through N1–C2–C3 delocalized π-cloud, with the highest contribution coming from the C3 atom of **2** (Ni–C_{indole} = 2.49 Å; see Figure S49 in the Supporting Information). Successful geometry optimization of intermediate **A** showed a significant elongation of the Ni–$C_{carbene}$ bond by 0.8 Å (Ni–$C_{carbene}$ = 1.87 Å; see the Supporting Information[15g]), when compared to that in **Int-3a** (1.79 Å), providing evidence for weakening of the Ni–$C_{carbene}$ bond. In

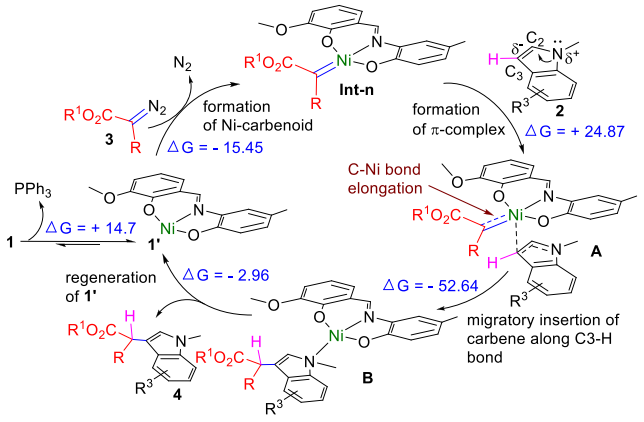

Figure 3. Proposed mechanism for the C3 functionalization of **2**. ΔG^{298} values are given in units of kcal/mol and calculated for R = H, R^1 = Et, R^3 = H, *n* = **3a**, **Int-3a**.

the next step, migratory insertion of the carbenoid (:C(R)-CO_2R^1) occurs from the Ni center to the C3 atom of **2**, leading to the formation of intermediate **B**. This process was determined to be highly exergonic. Finally, the decoordination of product **4** from the Ni center occurs, releasing the expected C3-functionalized product **4** and the monomeric intermediate **1′**. **1′** further reacts with diazoester **3** to regenerate the **Int-*n*** and participate in the next catalytic cycle.

The proposed mechanism for cyclopropanation is depicted in Figure 4. Once the **Int-3a** is generated *in situ*, the formation

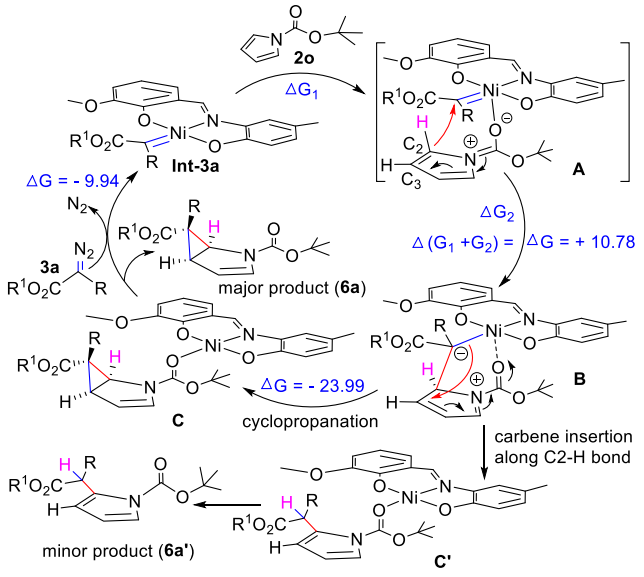

Figure 4. Proposed mechanism and model for stereocontrol of cyclopropanation. R = H, R^1 = Et. ΔG^{298} values are given in units of kcal/mol.

of intermediate **A** (see the Supporting Information[15h]) occurs upon coordination of the lone pair of O_{co} of the Boc group. However, this intermediate could not be optimized theoretically. In the next step, the $C_{carbene}$ of the Ni–$C_{carbene}$ bond of **A** accepts the nucleophilic attack[14] (to its LUMO) from the C2 carbon of **2** (see the Supporting Information[15i]) to produce the six-membered metallacycle **B**, for which the geometry could be successfully optimized (see the Supporting Information[15j]). This zwitterionic intermediate **B** with a longer

https://dx.doi.org/10.1021/acs.orglett.0c02138
Org. Lett. XXXX, XXX, XXX–XXX

Ni−$C_{carbene}$ bond (2.00 Å; see the Supporting Information[15j]) either can form the cyclopropane ring (isolated as the major product) from the same surface by attacking back at the C3 atom or can collapse into the C2−H bond functionalization product (in a few cases, isolated as the minor product). We assume that the formation of this zwitterionic intermediate, having only the top phase available, because of the sterically crowded bottle phase, is crucial for the observed *exo*-diastereoselectivity of the cyclopropanated products. Finally, dissociation of the weakly bonded product (**6**) from the Ni center of **C** occurs, regenerating the monomeric active catalyst **1′**, followed by the binding of the diazoester to produce **Int-3a** for the next catalytic cycle.

In conclusion, we have developed an efficient, cost-effective Ni(II)-phosphene (**1**)-catalyzed chemodivergent C−H functionalization and cyclopropanation of aromatic heterocycles with excellent regioselectivity and diastereoselectivity. The overall process is atom-economic, highly functional-group-tolerant, and provides an efficient route to generate functionalized indoles, pyrroles, and furans in good yields and selectivity. On the basis of experimental results and theoretical calculations, we have proposed that, mechanistically, the inherent inductive nature of the DG attached to the heteroatom of the aromatic heterocycle plays a crucial role in the unique chemodivergence.

■ ASSOCIATED CONTENT

Supporting Information

The Supporting Information is available free of charge at https://pubs.acs.org/doi/10.1021/acs.orglett.0c02138.

Syntheses of complex **1**, compounds **2**−**6**; NMR; UV-vis; mass spectrometric analysis; single-crystal X-ray diffraction of complex **1** and representatives of compounds **4**, **5**, and **6**; computational details; spectral data for **1**−**6**; copies of ^{1}H, ^{13}C, and ^{31}P NMR spectra (PDF)

Accession Codes

CCDC 1896711−1896714, 1922563, 1922565, and 1922566 contain the supplementary crystallographic data for this paper. These data can be obtained free of charge via www.ccdc.cam.ac.uk/data_request/cif, or by emailing data_request@ccdc.cam.ac.uk, or by contacting The Cambridge Crystallographic Data Centre, 12 Union Road, Cambridge CB2 1EZ, UK; fax: +44 1223 336033.

■ AUTHOR INFORMATION

Corresponding Authors

Sudipta Roy − *Department of Chemistry, Indian Institute of Science Education and Research (IISER), Tirupati 517507, India;* orcid.org/0000-0002-5883-4329; Email: roy.sudipta@iisertirupati.ac.in

Kartik Chandra Mondal − *Department of Chemistry, Indian Institute of Technology Madras, Chennai 600036, India;* Email: csdkartik@iitm.ac.in

Authors

Ekta Nag − *Department of Chemistry, Indian Institute of Science Education and Research (IISER), Tirupati 517507, India;* orcid.org/0000-0003-4490-4207

Sai Manoj N. V. T. Gorantla − *Department of Chemistry, Indian Institute of Technology Madras, Chennai 600036, India;* orcid.org/0000-0001-7315-6354

Selvakumar Arumugam − *Department of Chemistry, Indian Institute of Technology Madras, Chennai 600036, India*

Aditya Kulkarni − *Department of Chemistry, Indian Institute of Science Education and Research (IISER), Tirupati 517507, India;* orcid.org/0000-0002-0735-4851

Complete contact information is available at: https://pubs.acs.org/10.1021/acs.orglett.0c02138

Notes

The authors declare no competing financial interest.

■ ACKNOWLEDGMENTS

S.R. and K.C.M. gratefully acknowledge SERB, New Delhi for their respective ECR grants (No. ECR/2016/000733 for S.R.; No. ECR/2016/000890 for K.C.M.). E.N. thanks IISER, Tirupati and A.K. thanks KYPY for financial support. S.M.N.V.T.G. and S.A. thank CSIR for SRF. We thank Prof. K. N. Ganesh (Director, IISER Tirupati) and Prof. M. S. Krishnan (IIT Madras) for their support to complete this work.

■ REFERENCES

(1) Mizuno, A.; Matsui, K.; Shuto, S. A Strategy Based on the Structural Features of Cyclopropane. *Chem. - Eur. J.* **2017**, *23*, 14394.

(2) (a) Bhardwaj, V.; Gumber, D.; Abbot, V.; Dhiman, S.; Sharma, P. A Resourceful Small Molecule in Key Medicinal Hetero-aromatics. *RSC Adv.* **2015**, *5*, 15233. (b) Kirillova, M. S.; Muratore, M. E.; Dorel, R.; Echavarren, A. M. Concise Total Synthesis of Lundurines A-C Enabled by Gold Catalysis and a Homodienyl Retro-Ene/Ene Isomerization. *J. Am. Chem. Soc.* **2016**, *138*, 3671. (c) Xu, H.; Li, Y. P.; Cai, Y.; Wang, G. P.; Zhu, S. F.; Zhou, Q. L. Highly Enantioselective Copper- and Iron-Catalyzed Intramolecular Cyclopropanation of Indoles. *J. Am. Chem. Soc.* **2017**, *139*, 7697.

(3) (a) Joucla, L.; Djakovitch, L. Transition Metal-Catalyzed, Direct and Site-Selective N1-, C2- or C3-Arylation of the Indole Nucleus: 20 Years of Improvements. *Adv. Synth. Catal.* **2009**, *351*, 673. (b) Gao, X.; Wu, B.; Huang, W.-X.; Chen, M.-W.; Zhou, Y.-G. Enantioselective Palladium-Catalyzed C-H Functionalization of Indoles Using an Axially Chiral 2,2′-Bipyridine Ligand. *Angew. Chem., Int. Ed.* **2015**, *54*, 11956. (c) Loup, J.; Zell, D.; Oliveira, J. C. A.; Keil, H.; Stalke, D.; Ackermann, L. Asymmetric Iron-Catalyzed C−H Alkylation Enabled by Remote Ligand *meta*-Substitution. *Angew. Chem.* **2017**, *129*, 14385. (d) Pilsl, L. K. A.; Ertl, T.; Reiser, O. Enantioselective Three-Step Synthesis of Homo-*β*-proline: A Donor-Acceptor Cyclopropane as Key Intermediate. *Org. Lett.* **2017**, *19*, 2754. (e) Pesciaioli, F.; Dhawa, U.; Oliveira, J. C. A.; Yin, R.; John, M.; Ackermann, L. Enantioselective Cobalt(III)-Catalyzed C−H Activation Enabled by Chiral Carboxylic Acid Cooperation. *Angew. Chem., Int. Ed.* **2018**, *57*, 15425. (f) Özüduru, G.; Schubach, T.; Boysen, M. M. K. Enantioselective Cyclopropanation of Indoles: Construction of All-Carbon Quaternary Stereocenters. *Org. Lett.* **2012**, *14*, 4990. (g) Li, Y. P.; Li, Z. Q.; Zhu, S. F. Recent Advances in Transition-Metal-Catalyzed Asymmetric Reactions of Diazo Compounds with Electron-Rich (Hetero-) Arenes. *Tetrahedron Lett.* **2018**, *59*, 2307.

(4) (a) Gogoi, A.; Guin, S.; Rout, S. K.; Patel, B. K. Copper-Catalyzed Synthesis of 3-Aroylindoles via a sp^3 C-H Bond Activation Followed by C-C and C-O Bond Formation. *Org. Lett.* **2013**, *15*, 1802. (b) Dutta, P. K.; Chauhan, J.; Ravva, M. K.; Sen, S. Directing Group-Assisted Manganese-Catalyzed Cyclopropanation of Indoles. *Org. Lett.* **2019**, *21*, 2025. (c) Ghorai, J.; Chaitanya, M.; Anbarasan, P. Cp*Co(III)-Catalyzed Selective Alkylation of C-H Bonds of Arenes and Heteroarenes with *α*-diazocarbonyl compounds. *Org. Biomol. Chem.* **2018**, *16*, 7346. (d) Li, Z.; Shi, Z.; He, C. Addition of

Heterocycles to Electron Deficient Olefins and Alkynes Catalyzed by Gold(III). *J. Organomet. Chem.* **2005**, *690*, 5049. (e) Jackson, R. W.; Manske, R. H. The Reaction Products of Indoles with Diazoesters. *Can. J. Res.* **1935**, *13b*, 170. (f) Gibe, R.; Kerr, M. A. Convenient Preparation of Indolyl Malonates via Carbenoid Insertion. *J. Org. Chem.* **2002**, *67*, 6247.

(5) For enzyme-catalyzed cyclopropanation, see: (a) Coelho, P. S.; Brustad, E. M.; Kannan, A.; Arnold, F. H. Olefin Cyclopropanation via Carbene Transfer Catalyzed by Engineered Cytochrome P450 Enzymes. *Science* **2013**, *339*, 307. (b) Carminati, D. M.; Fasan, R. Stereoselective Cyclopropanation of Electron-Deficient Olefins with a Cofactor Redesigned Carbene Transferase Featuring Radical Reactivity. *ACS Catal.* **2019**, *9*, 9683. For enzyme-catalyzed C-H functionalization of indoles, see: (c) Brandenberg, O. F.; Chen, K.; Arnold, F. H. Directed Evolution of a Cytochrome P450 Carbene Transferase for Selective Functionalization of Cyclic Compounds. *J. Am. Chem. Soc.* **2019**, *141*, 8989.

(6) (a) Ji, Y.; Plata, R. E.; Regens, C. S.; Hay, M.; Schmidt, M.; Razler, T.; Qiu, Y.; Geng, P.; Hsiao, Y.; Rosner, T.; Eastgate, M. D.; Blackmond, D. G. Mono-Oxidation of Bidentate Bis-phosphines in Catalyst Activation: Kinetic and Mechanistic Studies of a Pd/Xantphos-Catalyzed C-H Functionalization. *J. Am. Chem. Soc.* **2015**, *137*, 13272. (b) Rull, S. G.; Álvarez, E.; Fructos, M. R.; Belderrain, T. R.; Pérez, P. J. The Elusive Palladium-Diazo Adduct Captured: Synthesis, Isolation and Structural Characterization of [(ArNHC-PPh_2)Pd(η^2-$N_2C(Ph)CO_2Et$)]. *Chem. - Eur. J.* **2017**, *23*, 7667.

(7) Carlsen, R.; Wohlgemuth, N.; Carlson, L.; Ess, D. H. Dynamical Mechanism may Avoid High-Oxidation State Ir(V)-H Intermediate and Coordination Complex in Alkane and Arene C-H Activation by Cationic Ir(III) Phosphine. *J. Am. Chem. Soc.* **2018**, *140*, 11039.

(8) For Group-VI-phosphene complexes, see: (a) Fürstner, A.; Fürstner, A.; Picquet, M.; Bruneau, C.; Dixneuf, P. H. Cationic Ruthenium Allenylidene Complexes as a New Class of Performing Catalysts for Ring Closing Metathesis. *Chem. Commun.* **1998**, *12*, 1315. (b) Dorta, R.; Kelly, R. A., III; Nolan, S. P. Cross Metathesis Allowing the Conversion of a Ruthenium Indenylidene Complex into Grubbs' Catalyst. *Adv. Synth. Catal.* **2004**, *346*, 917.

(9) (a) Liu, K.; Xu, G.; Sun, J. Gold-Catalyzed Stereoselective Dearomatization/Metal-Free Aerobic Oxidation: Access to 3-Substituted Indolines/Oxindoles. *Chem. Sci.* **2018**, *9*, 634 and ref 3 therein. (b) Ciszewski, Ł. W.; Durka, J.; Gryko, D. Photocatalytic Alkylation of Pyrroles and Indoles with α-Diazo Esters. *Org. Lett.* **2019**, *21*, 7028. (c) Jurberg, I. D.; Davies, H. M. L. Blue Light-Promoted Photolysis of Aryldiazoacetates. *Chem. Sci.* **2018**, *9*, 5112. (d) Huang, X.; Webster, R. D.; Harms, K.; Meggers, E. Asymmetric Catalysis with Organic Azides and Diazo Compounds Initiated by Photoinduced Electron Transfer. *J. Am. Chem. Soc.* **2016**, *138*, 12636.

(10) Saha, S.; Jana, S.; Gupta, S.; Ghosh, A.; Nayek, H. P. Syntheses, Structures and Biological Activities of Square Planar Ni(II), Cu(II) Complexes. *Polyhedron* **2016**, *107*, 183.

(11) Parr, R. G.; Szentpály, L. v.; Liu, S. Electrophilicity Index. *J. Am. Chem. Soc.* **1999**, *121*, 1922.

(12) Khade, R. L.; Zhang, Y. Catalytic and Biocatalytic Iron Porphyrin Carbene Formation: Effects of Binding Mode, Carbene Substituent, Porphyrin Substituent, and Protein Axial Ligand. *J. Am. Chem. Soc.* **2015**, *137*, 7560.

(13) See: (a) Figure S41 in the Supporting Information.

(14) Vargas, D. A.; Tinoco, A.; Tyagi, V.; Fasan, R. Myoglobin-Catalyzed C-H Functionalization of Unprotected Indoles. *Angew. Chem., Int. Ed.* **2018**, *57*, 9911.

(15) See: (a) Tables S5 and S6; and Figure S40 and 43 in the Supporting Information. (b) Figure S41 in the Supporting Information, indicated by green color. (c) Table S7 and Figure S53 in the Supporting Information. (d) Figures S40, S42 and S44 in the Supporting Information. (e) Table S8; Figures S64 and S65 in the Supporting Information. (f) Figure S40 in the Supporting Information. (g) Figure S49 in the Supporting Information. (h) Figure S44 in the Supporting Information. (i) Table S7 in the Supporting Information. (j) Figure S50 in the Supporting Information.

(16) See page S77, Table S5, and Figures S53 and S64 in the Supporting Information.

https://dx.doi.org/10.1021/acs.orglett.0c02138
Org. Lett. XXXX, XXX, XXX−XXX